

Article

Experimental Dynamic Impact Factor Assessment of Railway Bridges through a Radar Interferometer

Massimiliano Pieraccini ^{1,*} , Lapo Miccinesi ¹ , Ali Abdorazzagh Nejad ² and Azadeh Naderi Nejad Fard ²

¹ Department of Information Engineering, University of Florence, Via Santa Marta, 3 50139 Firenze, Italy; lapo.miccinesi@unifi.it

² GeoRAYAN Ltd. Unit 4, No 6, Yas Alley, Yas St., Alikhani St., South Shiraz St., Tehran 1436953859, Iran; razagh@georayan.com (A.A.N.); a.naderi@georayan.com (A.N.N.F.)

* Correspondence: massimiliano.pieraccini@unifi.it

Received: 9 August 2019; Accepted: 20 September 2019; Published: 21 September 2019



Abstract: The dynamic impact factor (IM) is a widely accepted parameter to account for the effect of vehicles on bridges. An accurate evaluation of this IM is of paramount importance in bridge engineering, both for designing safe and economical new bridges, and for the assessment of the existing ones. At the state of the art, the current procedure for the experimental assessment of the IM of a bridge relies upon the deployment of a sensor network. The aim of this article is to propose the use of a remote sensor, the interferometric radar, for assessing the IM without the deployment of any sensor on the bridge, with evident advantages in terms of cost, time and safety of the workers. Two different case studies of bridges in Northern Iran are reported. In both cases the interferometric radar has been demonstrated an effective and reliable measurement equipment for this kind of in-field assessment.

Keywords: bridge monitoring; health structure monitoring; impact factor; radar; remote sensing; sensor

1. Introduction

It is well known that moving vehicles will exert a dynamic impact effect upon bridges, namely, the increment from the static load effect [1]. The use of the dynamic impact factor (IM) to account for the effect of vehicles has been widely accepted in bridge engineering. Accurate evaluation of the IM will lead to safe and economical designs for new bridges and provide valuable information for the condition assessment and management of the existing ones.

Many highway and rail bridges still in service have been designed back when vehicles' speeds were considerably lower. So extensive measurement campaigns have to be performed for updating the current speed limits, thus maintaining the safety of the bridges [2,3]. Furthermore, the modern high-speed trains pose serious challenges to bridge design and maintenance in terms of the dynamic load they have to be able to bear. Careful analyses and experimental studies have been performed about it [4–6].

The standard procedure for the experimental assessment of the IM of a bridge relies on the deployment of a sensor network, including strain gauges, accelerometers and the linear variable differential transformer (LVDT) for detecting the displacement in several points [7–10]. Fiber optic sensors [11] and GPS sensors [12] can be also used. Although the most recent contact sensors can operate in a wireless manner [13], their installation is again the most time consuming and expensive operation. Furthermore, the sensors have to be installed in points that are often difficult to access, and thus the safety of the involved workers can be a serious concern.

For these reasons, a remote equipment able to assess the IM at a distance without any installation of sensors on the structure of the bridge can be of great interest in engineering practice.

Both laser vibrometers [14] and vision-based sensors [15] could be used for detecting the effects of dynamic loads upon bridges, but the laser vibrometer is equipment that is not easily deployable in field, and the accuracy of the vision-based sensors are just at the limit for this kind of application.

The interferometric radar has been demonstrated to be an effective equipment for detecting the displacement of engineering structures like towers, bridges and buildings [16–18]. In particular, Pieraccini et al. [16] has demonstrated that radar detected displacement is in very good agreement with the displacement detected by a seismic accelerometer installed on the deck of a bridge under test.

Beben in 2013 [19] was the first to use an interferometric radar for assessing the IM of a railway culvert. With this aim he designed and set up special mechanical gauge for converting the vertical displacement of the culvert into the horizontal displacement of a Corner Reflector [20]. Indeed, the radar detects the component of the displacement in the view direction, that generally is not vertical, but oblique.

In this paper, for the first time, an interferometric radar is used for assessing the IM of two railway bridges without any additional equipment. As the first bridge (the Veresk Bridge, Savadkuh County, Mazandaran Province, Iran) crossed a narrow gorge, its geometry allowed the radar to be installed vertically under the main span, in order to detect only the vertical displacement. In this measurement geometry, a not too trivial question is which point of the bridge the radar effectively detects, as the field of view covers the whole arcade. This question is discussed in detail in this paper.

The second bridge (the Kaflan-Kuh Bridge in the East Azerbaijan Province, Iran) crossed a river, and the radar was installed close to a pillar, so it detected the oblique component of the displacement. In this measurement geometry, the critical point is how the oblique direction can affect the reliability of the results. In effect the standard procedure prescribes to use the vertical displacement for assessing the IM. Nevertheless, the measured data do not exhibit any systematic deviation of the results depending on the view angle.

These two acquisition modalities (vertical and oblique) are representative of the majority of cases where the interferometric radar can be used for IM assessment.

2. Materials and Methods

2.1. The Railway Bridges

The Veresk Bridge is a railway masonry arch bridge on the Veresk river in northern Iran. It has a central arch with a total length of 66 m and 10 small arches. Its central arch is 110 m height from the bottom of the valley. The bridge was built before World War II during the reign of Reza Shah, and it came into operation in 1936. Because of the difficult terrain, the bridge was an engineering challenge (see Figure 1).

During the Second World War, it was known as the Victory Bridge, because it was part of the Trans-Iranian Railway that helped the Allies to transport supplies needed by the USSR for preventing a German invasion. Since 1977 it has been part of National Heritage, and it is a popular touristic attraction [21]. It is still an essential part of the transport infrastructure. In the last years the Veresk Bridge has been the object of several simulated and experimental studies [3,10,22].

The Kaflan-Kuh Bridge is a railway bridge crossing the river Quezel Ozan in the North of Iran. It is a masonry bridge with two main spans 40 m large (see Figure 2).

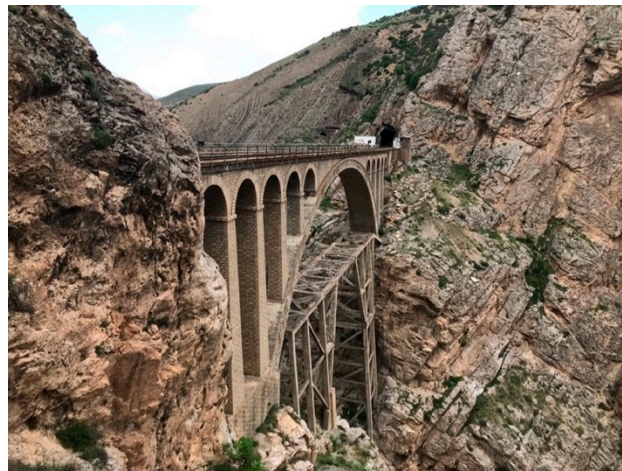


Figure 1. Veresk bridge, Northern Iran.

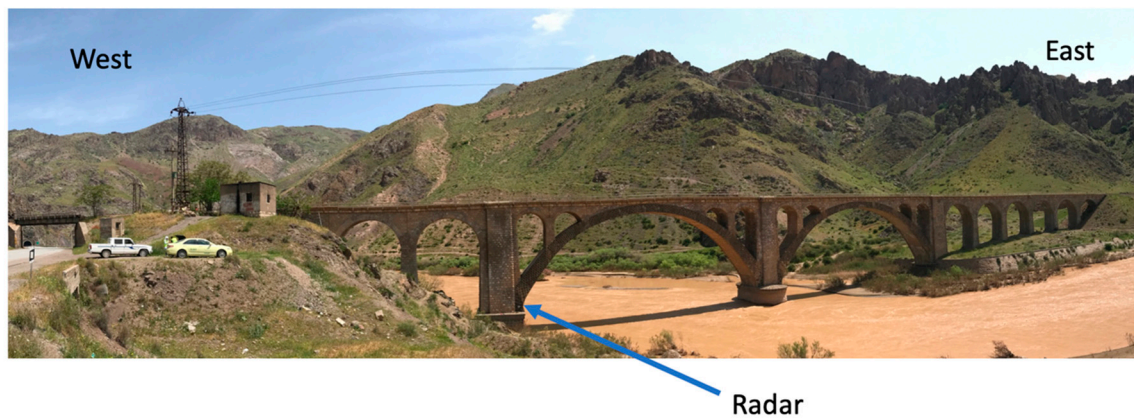


Figure 2. Kaflan-Kuh Bridge, Northern Iran.

2.2. The Radar Equipment

The radar that has been used during the measurement campaign reported in this article was a prototype operating in the Ku-band with bandwidth 300 MHz and a central frequency at 16.75 GHz [23]. It transmitted a Continuous Wave Step Frequency (CWSF) signal. The sweep time was 11.72 ms. The sweep time is even the sampling time of the structure under test. The number of stepped frequencies was 1,172. Therefore, the range resolution was 0.5 m, and the unambiguous range 586 m [24]. The transmitted power was 4 dBm, and the antennas (vertically polarized) had a gain of 24 dBi.

Figure 3 shows the radar installation at the Veresk Bridge. The equipment was deployed on the gorge 110 m below the central span of the bridge.



Figure 3. Radar deployment under the Veresk Bridge.

Figure 4 shows the radar installation at the Kaflan-Kuh Bridge. The equipment was on a tripod close to one of the pillars of the bridge.



Figure 4. Radar installation at the Kaflan-Kuh Bridge.

2.3. The Dynamic Impact Factor Definition

Despite its popularity and wide use in the engineering community, the definition of the concept of the impact factor (IM) is not as unambiguous as one might expect [25]. Generally speaking, the IM is the increment of stress (or equivalently, deflection) due to a dynamic load expressed as a fraction of an equivalent static load. Unfortunately, there is always a certain amount of ambiguity in the manner by which this increment is calculated. Figure 5 can help to clarify this point.

The red line represents the experimental deflection measured at one point of the bridge (typically at midspan). The blue line is the “static” response obtained by filtering the data with a suitable low pass filter. Its cut-off frequency (f_c) should be low enough to cut the dynamic contribution, but even high enough to follow the hypothetical displacement of the same load moving along the bridge “very slowly” (i.e., quasi-static). If the wheelbase (L) and the speed (v) of the carriage are known, a suitable cut-off frequency is:

$$f_c = \frac{2v}{L}, \quad (1)$$

With reference to Figure 5 the most common definition of IM is

$$IM = \frac{R}{R_f} - 1, \quad (2)$$

where R and R_f are respectively the maximum negative deflection of the not-filtered and filtered signal. The practical problem in the direct application of this definition is that it assumes that the zero-line of displacement is known. But in the real world, any sensor has its own drift, and the bridge is not an ideally elastic structure. Therefore, the identification of the zero-line is neither trivial nor unambiguous. As an example, often we note a small but evident lowering of the zero-line after the passage of the carriage that can persist even during the next passage. A more robust definition of IM has been discussed by Paultre [26]. It does not require the knowledge of the zero-line, and it takes into account both negative and positive deflections. With reference to Figure 5 this second definition of impact factor (IM_2) is

$$IM_2 = \frac{\Delta}{\Delta_f} - 1, \quad (3)$$

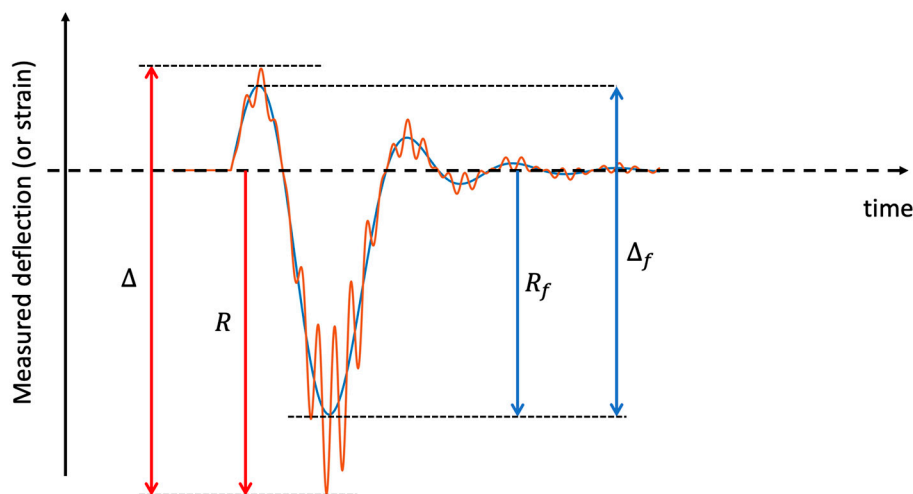


Figure 5. Deflection (or strain) in time of a point of a bridge excited by a dynamic load.

Unfortunately, these two definitions are not equivalent. The positive deflection is usually much smaller than the negative deflection, while the positive and negative increment can be of the same order of magnitude, so IM_2 can be up to twice IM . In the experimental part of this article we will assess the impact factor using both definitions.

3. Results

3.1. Veresk Bridge

At the Veresk Bridge, the radar was deployed at the bottom of the narrow gorge crossed by the bridge as shown in Figure 6. The radar was positioned exactly under the main span, so it detected only the vertical displacement.

A question that is worth discussing, is if the radar detects the displacement of the central point of the arcade, or includes all points of the arcade. In principle the radar cannot distinguish targets at the same range, so it could mix the signal of all points of the arcade at the same distance from the radar. Nevertheless, the curved shape of the arcade and the acquisition geometry excludes this possibility. The optical geometry prescribes that a ray close to the optical axis (the vertical direction in Figure 6), after specular reflection on a spherical mirror crosses the median point (F) between the mirror and the

center of the sphere (C). Therefore, if the specular reflection is predominant with respect to scattering, only the central point of the arc bridge reflects a signal that can be detected by the radar.

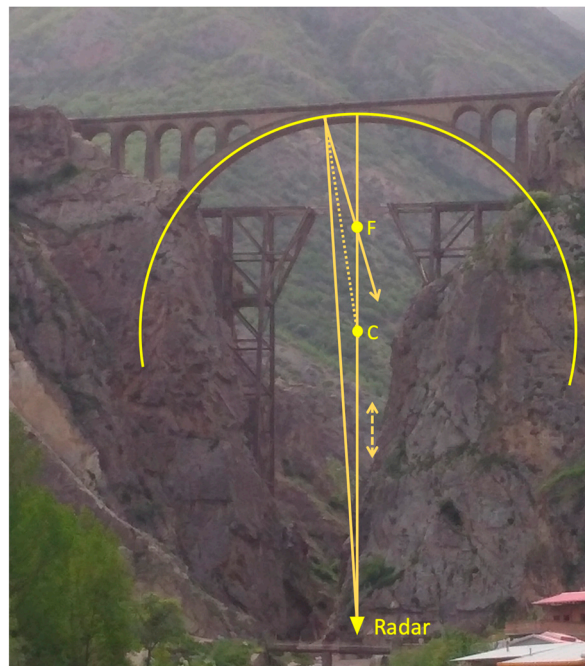


Figure 6. Geometry of the radar acquisition at Veresk Bridge.

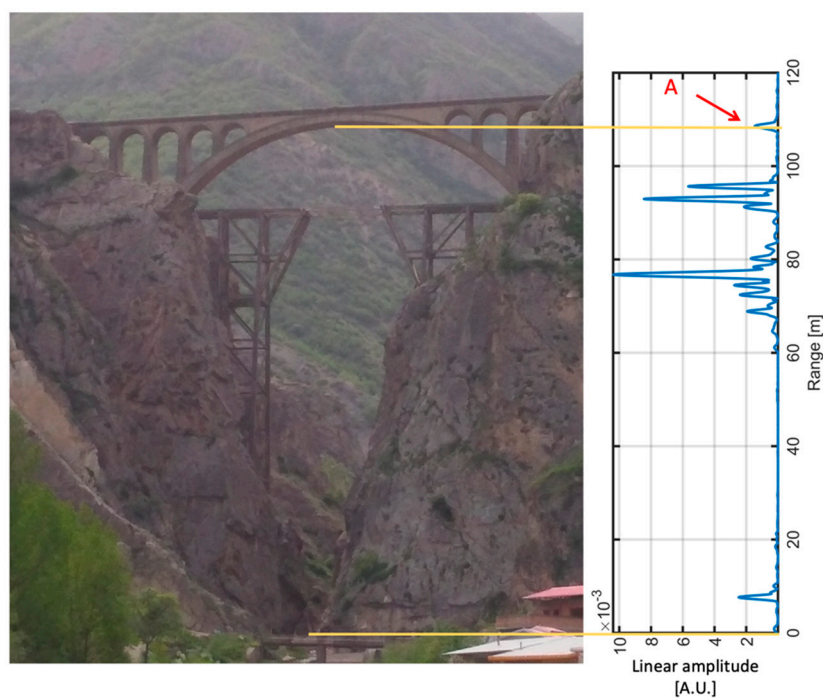


Figure 7. Picture of the Veresk Bridge and amplitude radar plot.

The radar provides a plot in range (distance from radar) with peaks related to targets at different ranges. The amplitude radar plot obtained at the Veresk Bridge is shown in Figure 7. The peak labeled with A corresponds to the bridge span about 100 m higher. Figure 8 shows the detected displacement at the point A during the passage of a cargo train. A few seconds before the arrival of the train, the central span goes up 0.5 mm, and then suddenly goes down 2.36 mm. This large displacement is due

to the weight of the locomotive. Aftermath, we see the passage of nine wagons that give displacements of about 0.5 mm. In order to estimate the IM, the cut-off frequency of the low pass filter has been set using the Equation (1), with $L = 14.17$ m and $v = 30$ km/h. The used low pass filter is a Butterworth with six poles implemented in Matlab [27].

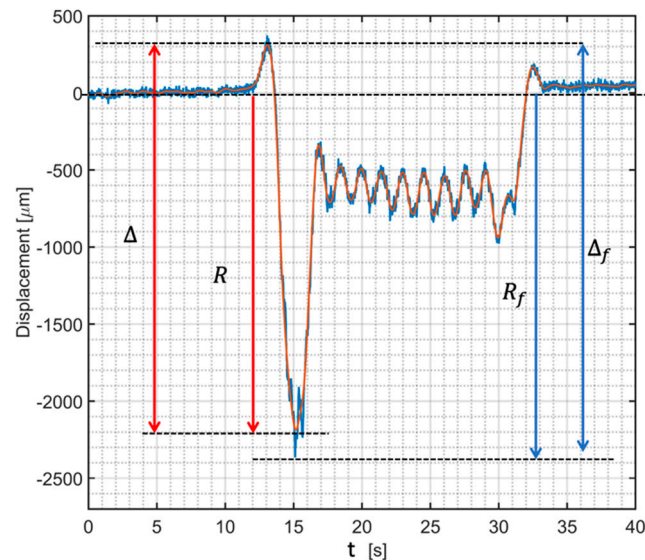


Figure 8. Displacement of the A-point of the plot in Figure 7 (the Veresk Bridge) during the passage of a cargo train.

The assessed dynamic impact factors (using both definitions) are $IM = 0.080$ and $IM_2 = 0.094$. These values are in agreement with the literature [3,22].

Just as reference, the American Association of State Highway and Transportation Officials (AASHTO) impact formula to calculate the dynamic loading of arch bridges [28] is:

$$IM = \frac{15.24}{LS + 38.1}, \quad (4)$$

with LS (in meters) length the span. For the Veresk Bridge, $LS = 66$ m, so $IM = 0.15$. By considering that Equation (4) is a rather conservative estimate, the measured IM appears consistent with it. As the IM given by AASHTO is a sort of safety margin in designing a bridge, a measured value lower than it can confirm the good health of a bridge.

3.2. Kaflan-Kuh Bridge

At the Kaflan-Kuh bridge, the radar was installed close to a pillar, as shown in Figure 4. The bridge has two main arcades, so both should be tested. Nevertheless, the aim of this measurement campaign was to demonstrate the capability of the technique in a realistic case study, so the test has been limited to the West Arcade.

The radar plot gives five clear peaks in correspondence to the higher part of the span, as sketched in Figure 9.

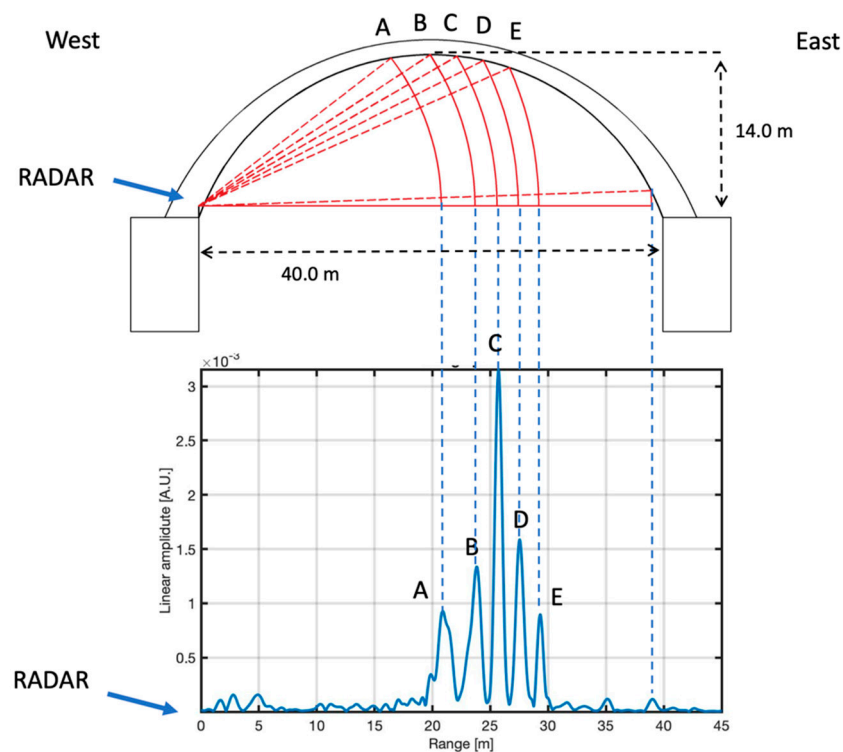


Figure 9. Radar plot in range as acquired at the Kaflan-Kuh Bridge.

In order to assess the impact factor of the bridge in a controlled test, a model EMD G22 locomotive was used. It is a popular diesel, weighing 70 t. Its wheelbase (L) is 13.26 m, and it can reach 150 km/h speed. The locomotive carried out seven passages back and forth at different speeds (see Table 1). Furthermore, the passages of two passenger trains were acquired. As the duration of the passage on a single point has been obtained by the displacement signal, the wheelbase (13.26 m) of the locomotive has been used for tuning the effective speed of each passage that resulted a little differently from the nominal value (especially for the passage at the lowest speed, 10 km/h). The wheelbases of the two passenger trains were not known, so we assumed them to be equal to the EMD G22 locomotive. Nevertheless, the obtained values are reasonable, as the speed limit on the bridge was 60 km/h.

Table 1. Train passages.

	Nominal Speed v_n (Km/h)	Measured Speed v_m (Km/h)	Direction	f_L (Hz)
Locomotive	70	74.41	East	3.03
Locomotive	70	72.30	West	2.82
Locomotive	50	44.19	East	1.73
Locomotive	50	48.88	West	1.92
Locomotive	30	34.25	East	1.34
Locomotive	30	32.33	West	1.27
Locomotive	10	19.72	East	0.77
Passenger 1	60	57.34	West	2.25
Passenger 2	60	64.51	East	2.53

As an example, Figure 10 shows the detected range displacement of the point C (see Figure 8) relative to the passage of the locomotive at 30 km/h (nominal speed) forward East.

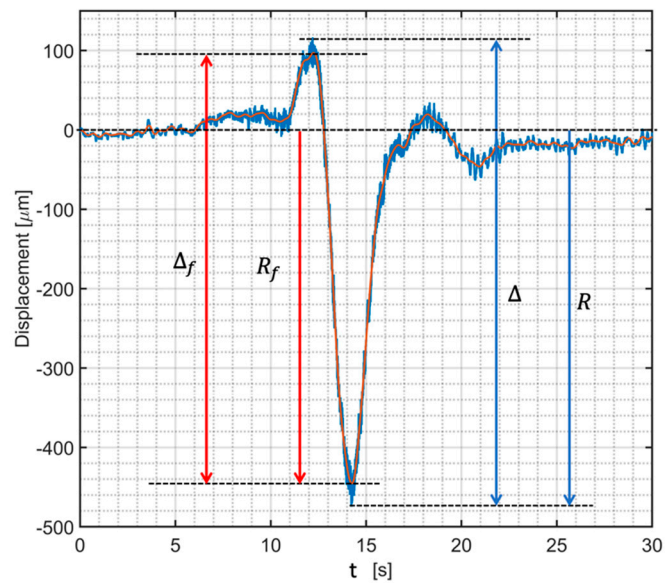


Figure 10. Detected range displacement of the point C (see Figure 8) relative to the passage of the locomotive at 30 km/h (nominal speed) forward East.

In the displacement signal of the passenger trains (Figure 11) it is possible to distinguish the locomotive (the first peak) and the wagons.

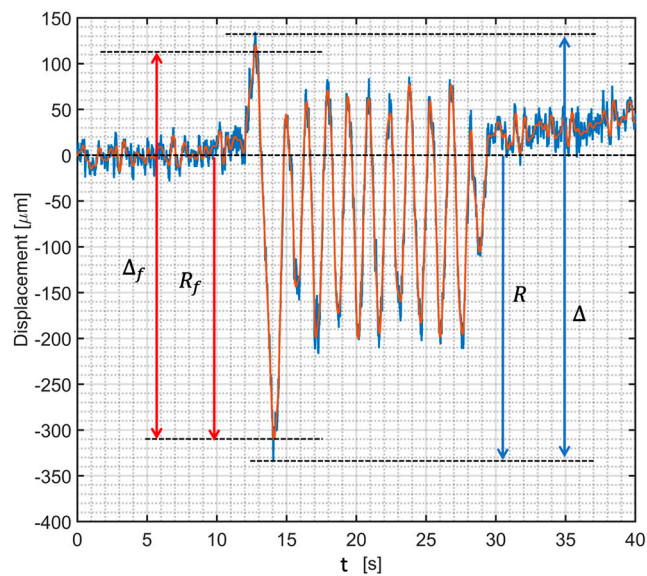


Figure 11. Detected range displacement of the B-point during the passage of a passenger train at 60 km/h (nominal speed) forward East.

The graph in Figure 12 shows the IM calculated for all the passages of all trains in all the points (A, B, C, D, E). For each speed the five values correspond to the five peaks (A, B, C, D, E) in the radar plots.

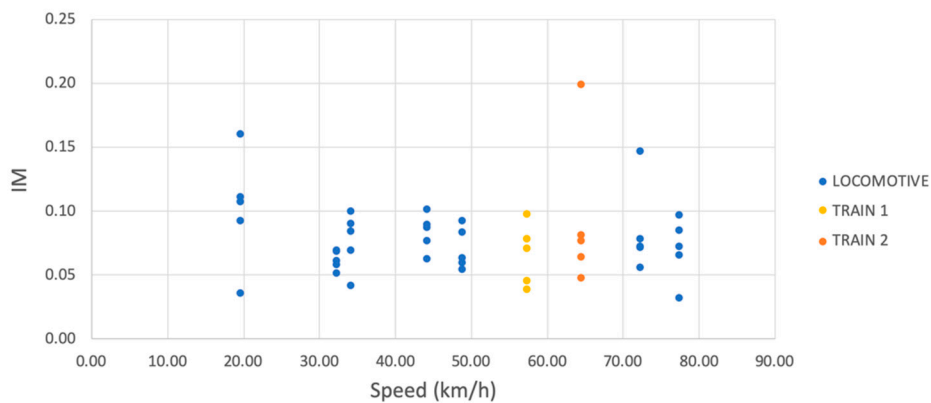


Figure 12. Impact factor (IM) calculated for all of the passages of all trains in all the points.

The measured IM values can appear rather scattered, but this is in agreement with the experimental results reported the literature [6,10,19,29].

A possible critical point of the geometry depicted in Figure 9 is how much the oblique direction can affect the reliability of the results. In effect, the standard procedure prescribes the use of the vertical displacement for assessing the IM. With this aim, Figure 13 shows the mean values of IM calculated for each of the five measurement points. The IM appears rather constant for different points. The standard deviation is 0.018.

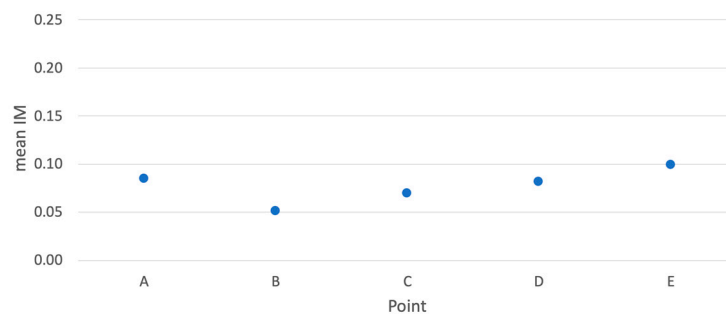


Figure 13. Mean IM calculated for each measurement point on the lower deck.

The plot in Figure 14 is obtained by averaging the five values for each speed. The IM appears rather constant at different speeds, at least up to about 80 km/h. This is consistent with the literature [30,31]. Therefore, it can be stated that $IM = 0.075$ in the considered speed range.

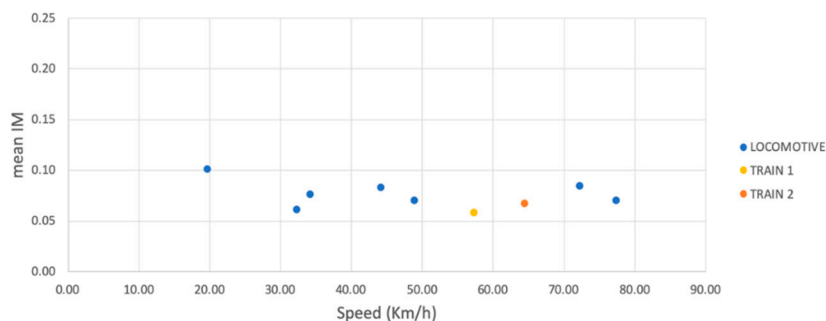


Figure 14. IM calculated, averaging the values of the five points on the span for each speed.

As mentioned above, the definition of IM that takes into account both the negative and positive deflection is experimentally more robust. For this reason, the impact factor has also been calculated using this second definition (IM_2). The graph in Figure 15 shows the IM_2 calculated for all the passages

of all trains in all the points (A, B, C, D, E). For each speed the five values correspond to the five peaks (A, B, C, D, E) in the radar plots.

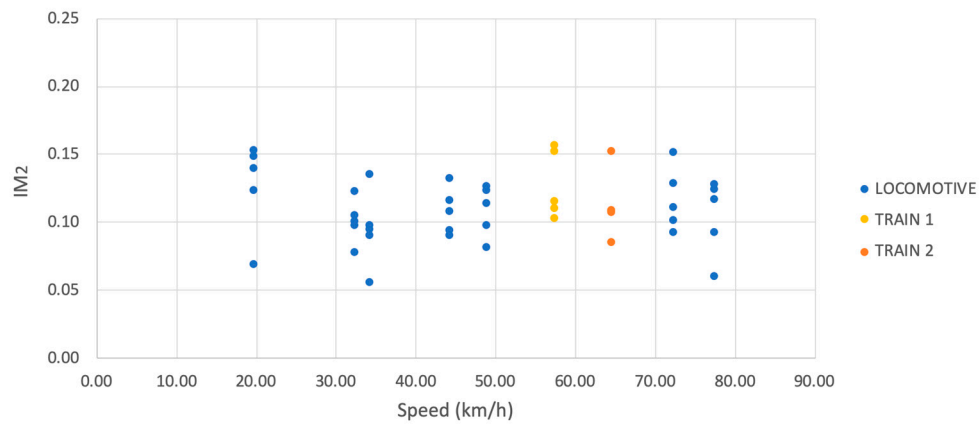


Figure 15. IM_2 calculated for all of the passages of all trains in all the points.

Figure 16 shows the mean values of IM_2 calculated for each of the five measurement points. The IM_2 (as previously noted for IM) appears rather constant in different points. The standard deviation is 0.016.

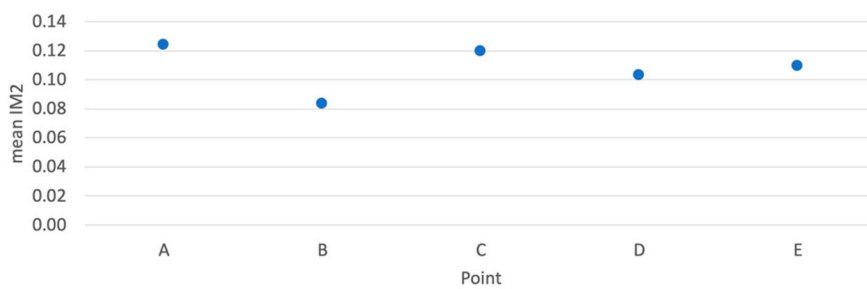


Figure 16. Mean IM_2 for each measurement point on the lower deck.

The graph in Figure 17 shows the averaged values.

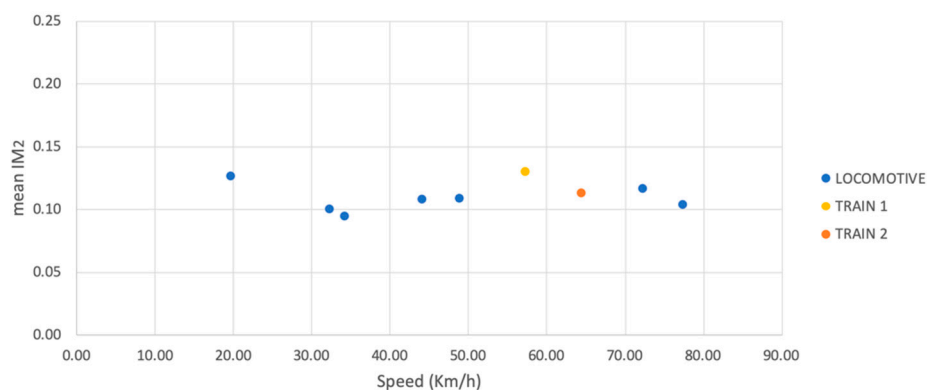


Figure 17. IM_2 calculated averaging the values of the five points on the span for each speed.

As expected, the values of IM_2 are a bit higher than the IM calculated with the most common definition. Even IM_2 is rather constant at different speeds, therefore it can be stated that $IM = 0.111$ in the considered speed range.

The (conservative) formula of the American Association of State Highway and Transportation Officials (AASHTO) for calculating the dynamic loading of arch bridges [29] gives $IM = 0.195$, that is consistent with the measured values.

4. Discussion

A couple of open questions about the use of this equipment for dynamic impact factor assessment have been addressed. The first one is relative to the measurement geometry of the first case study: A bridge crossing a deep gorge. In this case, a nontrivial question is which point of the bridge the radar effectively detects, as the field of view covers the whole arcade. In principle, the radar cannot distinguish targets at the same range, so it could mix the signal of all points of the arcade at the same distance from the radar. Nevertheless, the curved shape of the arcade excludes this possibility. Indeed, as the specular reflection is predominant with respect to scattering, only the central point of the arc bridge reflects a signal that can be detected by the radar.

The open question addressed in this article is relative to the second case study in which the radar was installed close to a pillar detecting the oblique component of the displacement. In this measurement geometry, the critical point is how the oblique direction can affect the reliability of the results. In effect the standard procedure prescribes a use of the vertical displacement for assessing the IM. Nevertheless, the measured data have not shown any significant systematic deviation of the results depending on the view angle.

5. Conclusions

An interferometric radar has been successfully used for assessing the dynamic impact factor of railway bridges both in controlled tests (with dynamic load of known weight and speed) and in operating conditions (with cargo or passenger trains). This sensor is able to operate at a safety distance (even at 100 m of distance in the case of the Veresk Bridge), without using scaffolding or cords for installing sensors on the deck.

Author Contributions: Methodology, M.P.; data acquisition and analysis, L.M.; campaign management, A.A.N. and A.N.N.F.; writing, M.P.; funding acquisition, A.A.N.

Funding: This research was funded by GeoRAYAN Ltd.

Acknowledgments: The authors would like to thank the department of railway and technical structures of Iranian Railway Company, specially M. Zehtabian, M. Sharafeddin, and H. Ebrahimi for their valuable support and cooperation.

Conflicts of Interest: The authors declare no conflict of interest.

References

1. Deng, L.; Yu, Y.; Zou, Q.; Cai, C.S. State-of-the-art review of dynamic impact factors of highway bridges. *J. Bridge Eng.* **2015**, *20*, 04014080. [[CrossRef](#)]
2. Paeglite, I.; Paeglitis, A. The Dynamic Amplification Factor of the Bridges in Latvia. *Procedia Eng.* **2013**, *57*, 851–858. [[CrossRef](#)]
3. Ataei, S.; Miri, A. Investigating dynamic amplification factor of railway masonry arch bridges through dynamic load tests. *Constr. Build. Mater.* **2018**, *183*, 693–705. [[CrossRef](#)]
4. Frýba, L. A rough assessment of railway bridges for high speed trains. *Eng. Struct.* **2001**, *23*, 548–556. [[CrossRef](#)]
5. Xia, H.; Zhang, N. Dynamic analysis of railway bridge under high-speed trains. *Comput. Struct.* **2005**, *83*, 1891–1901. [[CrossRef](#)]
6. Youliang, D.; Gaoxin, W. Evaluation of dynamic load factors for a high-speed railway truss arch bridge. *Shock Vib.* **2016**, *2016*, 5310769. [[CrossRef](#)]
7. Flener, E.B.; Karoumi, R.; Sundquist, H. Field testing of a long-span arch steel culvert during backfilling and in service. *Struct. Infrastruct. Eng.* **2005**, *1*, 181–188. [[CrossRef](#)]

8. Kwasniewski, L.; Wekezer, J.; Roufa, G.; Li, H.; Ducher, J.; Malachowski, J. Experimental evaluation of dynamic effects for a selected highway bridge. *J. Perform. Constr. Facil.* **2006**, *20*, 253–260. [[CrossRef](#)]
9. Szurgott, P.; Wekezer, J.; Kwasniewski, L.; Siervogel, J.; Ansley, M. Experimental assessment of dynamic responses induced in concrete bridges by permit vehicles. *J. Bridge Eng.* **2010**, *16*, 108–116. [[CrossRef](#)]
10. Ataei, S.; Nouri, M.; Kazemiashtiani, V. Long-term monitoring of relative displacements at the keystone of a masonry arch bridge. *Struct. Control Health Monit.* **2018**, *25*, e2144. [[CrossRef](#)]
11. Majumder, M.; Gangopadhyay, T.K.; Chakraborty, A.K.; Dasgupta, K.; Bhattacharya, D.K. Fibre Bragg gratings in structural health monitoring—Present status and applications. *Sens. Actuators A Phys.* **2008**, *147*, 150–164. [[CrossRef](#)]
12. Yi, T.H.; Li, H.N.; Gu, M. Experimental assessment of high-rate GPS receivers for deformation monitoring of bridge. *Measurement* **2013**, *46*, 420–432. [[CrossRef](#)]
13. Moreu, F.; Kim, R.E.; Spencer, B.F., Jr. Railroad bridge monitoring using wireless smart sensors. *Struct. Control Health Monit.* **2017**, *24*, e1863. [[CrossRef](#)]
14. Nassif, H.H.; Gindy, M.; Davis, J. Comparison of laser Doppler vibrometer with contact sensors for monitoring bridge deflection and vibration. *NDT E Int.* **2005**, *38*, 213–218. [[CrossRef](#)]
15. Feng, D.; Feng, M.; Ozer, E.; Fukuda, Y. A vision-based sensor for noncontact structural displacement measurement. *Sensors* **2015**, *15*, 16557–16575. [[CrossRef](#)]
16. Pieraccini, M.; Fratini, M.; Parrini, F.; Atzeni, C.; Bartoli, G. Interferometric radar vs. accelerometer for dynamic monitoring of large structures: An experimental comparison. *NDT E Int.* **2008**, *41*, 258–264. [[CrossRef](#)]
17. Kuras, P.; Owerko, T.; Ortyl, Ł.; Kocierz, R.; Sukta, O.; Pradelok, S. Advantages of radar interferometry for assessment of dynamic deformation of bridge. In Proceedings of the 6th International Conference on Bridge Maintenance, Safety and Management (IABMAS 2012), Stresa, Lake Maggiore, Italy, 8–12 July 2012; pp. 885–891.
18. Pieraccini, M. Monitoring of civil infrastructures by interferometric radar: A review. *Sci. World J.* **2013**, *2013*, 8. [[CrossRef](#)] [[PubMed](#)]
19. Beben, D. Experimental Study on the Dynamic Impacts of Service Train Loads on a Corrugated Steel Plate Culvert. *J. Bridge Eng.* **2013**, *18*, 339–346. [[CrossRef](#)]
20. Beben, D. Application of the interferometric radar for dynamic tests of corrugated steel plate (CSP) culvert. *NDT E Int.* **2011**, *44*, 405–412. [[CrossRef](#)]
21. Niloufar, A.; Mahdavinjad, M.; Forsat, M. Interaction of natural landscape and modern Heritage in case of Veresk, IRAN. *Sci. Her. Voronezh State Univ. Archit. Civ. Eng.* **2016**, *32*, 70–91.
22. Rafiee-Dehkharghani, R.; Ghyasvand, S.; Sahebalzamani, P. Dynamic Behavior of Masonry Arch Bridge under High-Speed Train Loading: Veresk Bridge Case Study. *J. Perform. Constr. Facil.* **2018**, *32*, 04018016. [[CrossRef](#)]
23. Pieraccini, M.; Fratini, M.; Parrini, F.; Atzeni, C. Dynamic monitoring of bridges using a high-speed coherent radar. *IEEE Trans. Geosci. Remote Sens.* **2006**, *44*, 3284–3288. [[CrossRef](#)]
24. Dei, D.; Pieraccini, M.; Fratini, M.; Atzeni, C.; Bartoli, G. Detection of vertical bending and torsional movements of a bridge using a coherent radar. *NDT E Int.* **2009**, *42*, 741–747. [[CrossRef](#)]
25. Bakht, B.; Pinjarkar, S.G. Dynamic Testing of Highway Bridges—A Review. *Transp. Res. Rec.* **1989**, *1223*, 93–100.
26. Paultre, P.; Chaallal, O.; Proulx, J. Bridge dynamics and dynamic amplification factors—A review of analytical and experimental findings. *Can. J. Civ. Eng.* **1992**, *19*, 260–278. [[CrossRef](#)]
27. Taylor, F. *Digital Filters: Principles and Applications with MATLAB*; John Wiley & Sons: Hoboken, NJ, USA, 2011.
28. American Association of State Highway and Transportation Officials (AASHTO). *Standard Specifications for Highway Bridges*, 16th ed.; AASHTO: Washington, DC, USA, 1996.
29. Li, Y.; Cai, C.S.; Liu, Y.; Chen, Y.; Liu, J. Dynamic analysis of a large span specially shaped hybrid girder bridge with concrete-filled steel tube arches. *Eng. Struct.* **2016**, *106*, 243–260. [[CrossRef](#)]

30. Chang, D.; Lee, H. Impact factors for simple-span highway girder bridges. *J. Struct. Eng.* **1994**, *120*, 704–715. [[CrossRef](#)]
31. Yau, J.D.; Yang, Y.B.; Kuo, S.R. Impact response of high speed rail bridges and riding comfort of rail cars. *Eng. Struct.* **1999**, *21*, 836–844. [[CrossRef](#)]



© 2019 by the authors. Licensee MDPI, Basel, Switzerland. This article is an open access article distributed under the terms and conditions of the Creative Commons Attribution (CC BY) license (<http://creativecommons.org/licenses/by/4.0/>).